HYPERTHERMIA TREATMENT SIMULATION USING 3D OCTREE MESHES

André Valente

andre.valente@ifrj.edu.br

COPPE/Department of Civil Engineering, Federal University of Rio de Janeiro &
Instituto Federal de Educação, Ciência e Tecnologia do Rio de Janeiro

Leandro Di Bartolo

dibartolo@on.br

Observatório Nacional, Rio de Janeiro

Felipe Loureiro

felipe.loureiro@ufsj.edu.br

Departament of Thermal and Fluid Sciences, Federal University of São João Del Rei

Webe João Mansur

webe@coc.ufrj.br

COPPE/Department of Civil Engineering, Federal University of Rio de Janeiro

Abstract. *Hyperthermia treatment for cancer are becoming increasingly more common. However, the thermal ablation procedures have a main limiting factor: the correct increase of the temperature in the living tissue, which in some cases can cause undesirable effects such as irreversible damages in the healthy tissue. This paper presents the development of a FVM-based formulation using OcTree meshes that aims to simulate the hyperthermia treatment by injection of nanoparticles. A 3D linear Pennes' model is employed to simulate the heat transfer in blood perfused living tissues with a tumor. The OcTree mesh is used due to its simplicity in griding and, at the same time, allowing local refinement using a nonconforming mesh. A simple numerical example is analyzed, validating the proposed algorithm and showing the efficiency of the proposed scheme.*

Keywords: *Pennes bioheat model, Finite volume method, OcTree, Hyperthermia, Nanoparticles.*

1 INTRODUCTION

Hyperthermia and treatments using nanoparticles have emerged as a new frontier in cancer treatments (Minkowycz et al., 2012; Huang and Hainfeld, 2013). The number of studies are becoming increasingly more common. However, the thermal ablation procedures have a main limiting factor: the correct increase of the temperature in the living tissue, which in some cases can cause undesirable effects such as irreversible damages in the healthy tissue. The success of the treatment is to raise the temperature in the cancerous tissue above 43^oC for a specific period of time in a non–invasive manner. In this way, numerical and computational tools are increasingly used in simulations of hyperthermia treatment with the goal of predicting the temperature field and, thus, guide the specialist more precisely before the actual medical procedure or even in real time, e.g., observing the change in skin surface and using inverse problems to predict the internal temperature. This last case presupposes the use of a very efficient algorithm for the direct problem.

The number of researchers working on the application of numerical methods for the simulation of a variety of medical problems has experienced a growth in the last decades. Frequently, the models involve complex geometries with the adoption of methods capable of dealing with unstructured meshes. The most frequently used methods are the finite element method (FEM) (Zienkiewicz and Morgan, 1983) and the finite volume method (FVM) (Barth, 1992).

The procedures of generating unstructured meshes for complex geometries are still very time consuming and a topic of intensive research. This difficulty, however, can be minimized in parts by the use of OcTree meshes, which possess several advantages with respect to the use of computational resources and data structure. In the OcTree meshes, the description of complex geometries are accomplished by regular cubes (volumes) and the refinement takes place only in certain regions which need higher resolution (smaller volumes) while others can be described with larger volumes, giving rise to a nonconforming mesh. The use of sparse matrices as the OcTree mesh data structure allows the construction of simple and efficient discrete differential operators. This approach is widely used for modeling other phenomena such as fluid dynamics (Popinet, 2003), electromagnetism (Haber and Heldmann, 2007; Horesh and Haber, 2011) and seismic waves (Valente et al., 2015b).

Several researches have applied FVM to construct computational models from Pennes' equation in many different applications (Das and Mishra, 2013; Das et al., 2013; Das and Mishra, 2014; Gwon, 2015; Nóbrega and Coelho, 2017; Zhang, 2005). The FVM is very flexible to handle any type of control volume and any type of unstructured mesh. However, taking into account the mentioned previously, the use of OcTree meshes can be more efficient.

The present work develops a computational strategy through the use of FVM to solve the linear Pennes' bioheat transfer equation in three dimensions applying OcTree meshes. The technique presents a great reduction in the number of unknowns in the final system since regions with smooth solutions can be described with large control volumes, whereas in regions where there are high-gradient solutions or where complex geometries need to be accurately described, smaller volumes may be used. Therefore the use of computational memory and the processing time is greatly reduced. In addition, OcTree meshes like those used in this paper are easily constructed because they are treated as sparse matrices.

2 MATHEMATICAL MODEL FOR BIOHEAT CONDUCTION

Hyperthermia with nanoparticles can be used as a non-invasive treatment for destroying tumors in living tissue. The goal is to heat the tumor up to a temperature threshold above the normal physiological one in order to destroy its cells by necrosis while maintaining the damage of the healthy tissue as minimal as possible. This process can be mathematically modeled by considering bioheat equations that describe the heat transfer in living tissue. Among many different bioheat models, the well-known Pennes' equation is widely employed due to its simplicity and overall good agreement with experimental data. The Pennes' equation can be written as (Minkowycz, 2009):

$$-\nabla \cdot \mathbf{q} + W_b(\phi)c_b(\phi_a - \phi) + Q_m + Q_r = \rho c \frac{\partial \phi}{\partial t} \tag{1}$$

$$\mathbf{q} = -k\nabla\phi \tag{2}$$

$$\phi = \bar{\phi} \tag{3}$$

$$q_n = \bar{q} \tag{4}$$

$$\phi\left(\cdot, 0\right) = \phi_0 \tag{5}$$

where ϕ stands for the temperature field, and $\bar{\phi}$ and $\bar{q}$ are proper boundary conditions specified on the boundary to model the core body as well as the skin surface. The thermophysical properties are represented by k, ρ, c, c_b with subscript b denoting blood. In addition, ϕ_a denotes the arterial temperature, while Q_m and Q_r represent, respectively, the volumetric rate of metabolic heat generation and the volumetric rate of heat generation due to the external heat due to nanoparticles. Finally, the major parameter of Pennes' equation is the so-called blood perfusion denoted by W_b. In the above equation, the term that contains the blood perfusion is responsible for modeling the convective heat transfer between the tissue and the blood flow under the assumption of small capillaries and local thermal equilibrium.

After the injection of the nanoparticles, an external magnetic field is applied to excite the nanoparticles. The amount of heat generated is a consequence of the Brownian motion and Neel relaxation. In this work such a mechanism is simulated as an external heat source described by the following expression (Salloum et al., 2008)

$$Q_r = \sum_{i=1}^{n} A_i e^{-r_i^2/r_{i0}^2}, \tag{6}$$

where $r_i = \|\mathbf{x} - \mathbf{x}_i\|$ is the radial distance from the injection point i, r_{i0} is the distance covered by the heat generated, A_i is the maximum value of the volumetric heat generation rate, and n is the total number of injection points. The injection of a biocompatible base fluid with nanoparticles in several different places and with different concentrations allows a better treatment of tumors with irregular shapes, compromising minimally the healthy tissue.

3 NUMERICAL SCHEME

3.1 OcTree mesh generation

An OcTree mesh is represented by a sparse three-dimensional matrix $\mathbf{M}$, with dimensions $n_x \times n_y \times n_z = 2^a \times 2^b \times 2^c$, where its non-zero values are also powers of 2 (Haber and

Heldmann, 2007; Valente et al., 2015b). Let h be the grid spacing corresponding to one unit of the mesh, hence the total dimensions of the mesh are given by the dimensions of **M** multiplied by h. Then, the non-zero values of the mesh represent cubic volumes with edges given by the product of these values by h. In this paper, it is required that the OcTree mesh is balanced, i.e., the ratio between neighbors volumes edges must be 1/2, 1 or 2. Figure 1 illustrates a very small mesh with dimensions $2^3 \times 2^2 \times 2^2$ and its **M** matrix.

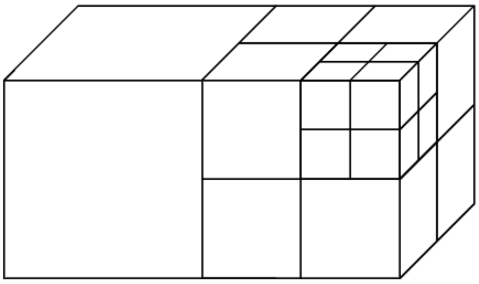

$$\mathbf{M}_{*,*,1} = \begin{pmatrix} 4&0&0&0&2&0&2&0 \\ 0&0&0&0&0&0&0&0 \\ 0&0&0&0&2&0&1&1 \\ 0&0&0&0&0&0&1&1 \end{pmatrix} \quad \mathbf{M}_{*,*,3} = \begin{pmatrix} 0&0&0&0&2&0&2&0 \\ 0&0&0&0&0&0&0&0 \\ 0&0&0&0&2&0&2&0 \\ 0&0&0&0&0&0&0&0 \end{pmatrix}$$

$$\mathbf{M}_{*,*,2} = \begin{pmatrix} 0&0&0&0&0&0&0&0 \\ 0&0&0&0&0&0&0&0 \\ 0&0&0&0&0&0&1&1 \\ 0&0&0&0&0&0&1&1 \end{pmatrix} \quad \mathbf{M}_{*,*,4} = \begin{pmatrix} 0&0&0&0&0&0&0&0 \\ 0&0&0&0&0&0&0&0 \\ 0&0&0&0&0&0&0&0 \\ 0&0&0&0&0&0&0&0 \end{pmatrix}$$

Figure 1: A small OcTree Mesh.

Concerning the OcTree mesh generation, a criterion that considers the proximity with interfaces, tumor boundaries, and sources is used. Due to practical purposes, it is considered first a fine regular mesh (a grid) will be used as input to generate the OcTree mesh. We apply a specific criterion on the input grid to coarse and set the elements of OcTree volumes, and generate **M**. Figure 3 shows an example of mesh (used in numerical example).

3.2 Discretization of differential operators

Let V_i be a regular cubic control volume with surface S_i surrounding node i originated from the discretization of the computational domain into n_v nonoverlapping control volumes by the OcTree method. The usual FVM when applied to Eq. (1) gives rise to the following integral statement:

$$\frac{1}{Vol\left(V_i\right)} \int\limits_{V_i} -\nabla \cdot \mathbf{q} d\Omega + W_b\left(\bar{\phi}_i\right)\left(c_b\right)_i \left(\left(\bar{\phi}_a\right)_i - \bar{\phi}_i\right) + \left(\bar{Q}_m\right)_i + \left(\bar{Q}_r\right)_i = \rho_i c_i \frac{\partial \bar{\phi}_i}{\partial t} \tag{7}$$

where $\bar{\bullet}_i = \frac{1}{Vol(V_i)} \int_{V_i} \bullet d\Omega$ stands for control volume average values. By considering the rectangular integral rule at node i, the overbar can be dropped since the average value is equal to the value at node i. The flux-balance approach (Dormy and Tarantola, 1995) is employed to deal with the divergent operator from the first term of Eq. (7). In this sense, after applying the Gauss theorem, we can write

$$Div(\boldsymbol{q}_i) = \frac{1}{Vol\left(V_i\right)} \int\limits_{V_i} -\nabla \cdot \mathbf{q} d\Omega = \frac{1}{Vol\left(V_i\right)} \int\limits_{S_i} -\mathbf{q} \cdot \mathbf{n}_i d\Gamma = \frac{1}{Vol\left(V_i\right)} \sum_{j=1}^{6} \int\limits_{F_j^i} -\mathbf{q} \cdot \mathbf{n}_j d\Gamma \tag{8}$$

where $F_j^i, j = 1...6$ denote the faces of the control volume with normal vectors $\mathbf{n}_j$.

The numerical scheme is construct using the $\mathbf{M}$ matrix previously defined, it is necessary to numbering all the n_v volumes and all the n_f faces. Then, we construct the following diagonal matrices: $\mathbf{V_o}$ with dimensions $n_v \times n_v$, where the elements are the volumes of V_i, and $\mathbf{F_o}$ with dimensions $n_f \times n_f$ where the elements are the edge dimensions of the faces F_i. Another matrix needs to be used, namely, the sparse matrix $\mathbf{N}$, with dimensions $n_v \times n_f$, that connects the volumes with their faces. Its elements are defined as $N_{i,j} = \pm 1$ if F_j belongs to V_i. If $\boldsymbol{q}$ is directed to the inside of the V_i, $N_{i,j} = +1$ and, if $\boldsymbol{q}$ is directed to the outside of the V_i, $N_{i,j} = -1$.

Using the matrices stated above, the discrete divergent operator and the discrete gradient operator are (Valente et al., 2015b)

$$\mathbf{DIV} = \frac{1}{h}\mathbf{V_o^{-1}NF_o^2}, \tag{9}$$

$$\mathbf{GRAD} = -\frac{1}{h}\mathbf{F_o^{-1}N^T}. \tag{10}$$

A simple example of the construction of the matrices for an OcTree mesh can be found in Valente et al. (2015a).

3.3 Spatial discretization

Using this discrete operators, the discretization of Pennes' equation is readily carried out. In the same way, the metabolic heat generation and the heat source generated by the nanoparticles in the control volumes of the mesh are represented, respectively, by the vectors $\mathbf{q}_m$ and $\mathbf{q}_r$ with dimensions $n_v \times 1$, obtained considering their values at the center of each control volume. We define new diagonal matrices, namely, the $\mathbf{C}$ and $\bar{\mathbf{C}}(\boldsymbol{\phi})$ matrices with dimensions $n_v \times n_v$, where $C_{i,i} = (\rho_i c_i)^{-1}$ and $\bar{C}_{i,i} = W(\phi_i)(c_b)_i/(\rho_i c_i)$ for each V_i; the $\mathbf{L}$ matrix with dimensions $n_f \times n_f$, where $L_{i,i}$ is the harmonic mean of the thermal conductivities of neighboring volumes that have F_i as face. Finally, using the discrete operators, we can write

$$(\mathbf{CV_o^{-1}NF_o^2LF_o^{-1}N^t})\boldsymbol{\phi} + \bar{\mathbf{C}}(\boldsymbol{\phi})(\boldsymbol{\phi}_a - \boldsymbol{\phi}) + \mathbf{Cq}_m + \mathbf{Cq}_r = \frac{\partial \boldsymbol{\phi}}{\partial t}. \tag{11}$$

Writing the matrix $\mathbf{CV_o^{-1}NF_o^2LF_o^{-1}N^t} = \mathbf{Y}$, the products $\mathbf{Cq}_m = \mathbf{m}$ and $\mathbf{Cq}_r = \mathbf{r}$, Eq. (11) can be concisely rewritten as

$$\mathbf{Y}\boldsymbol{\phi} + \bar{\mathbf{C}}(\boldsymbol{\phi})(\boldsymbol{\phi}_a - \boldsymbol{\phi}) + \mathbf{m} + \mathbf{r} = \frac{\partial \boldsymbol{\phi}}{\partial t}, \tag{12}$$

where $\boldsymbol{\phi}$ is the unknown nodal temperature vector at the center of the control volumes with dimensions $n_v \times 1$.

3.4 Integration in time

In order to solve Eq. (12), we adopt explicit time-integration approach. To this end, first, the time interval of interest I is partitioned into N equal time steps, i.e., $[0, t_f] = \bigcup\limits_{k=0}^{N-1} [t_k, t_{k+1}]$

with $0 = t_0 < t_1 < \ldots < t_N = t_f$, $\Delta t = t_{k+1} - t_k = t_f/N$ and $t_{k+1} = (k+1)\,\Delta t$. In this way, the explicit scheme using the backward finite difference (Zienkiewicz and Morgan, 1983; Reddy, 2014) can be written as:

$$\boldsymbol{\phi}^{k+1} = \left(\mathbf{I} + \Delta t\mathbf{Y} - \Delta t\bar{\mathbf{C}}\left(\boldsymbol{\phi}^k\right)\right)\boldsymbol{\phi}^k + \Delta t\mathbf{R}^k \tag{13}$$

where $\mathbf{R}^k = \bar{\mathbf{C}}\left(\boldsymbol{\phi}^k\right)\boldsymbol{\phi}_a + \mathbf{m} + \mathbf{r}^k$ and $\boldsymbol{\phi}^k \equiv \boldsymbol{\phi}\left(t_k\right)$.

Due to the conditionally stability of the explicit approach, the time-step size for the FVM using an OcTree mesh is readily estimated bearing in mind the criterion of the standard finite difference method (FDM). In the FDM, under the assumption of a linear and isotropic medium, a stability criterion of the form $\frac{\Delta t}{\rho c}\left(\frac{3k}{h_{min}^2} + \frac{W_b c_b}{4}\right) \leq \frac{1}{2}$ must be satisfied to assure stable results, where h_{min} is the minimum edge size of the whole mesh (Reis et al., 2016).

4 NUMERICAL EXAMPLE

Here, the proposed methodology is applied to a three-dimensional hyperthermia problem and the results are compared to those of the standard FDM (using regular cubic grid). The hyperthermia process is simulated in a computational domain of length $0.1 \times 0.1 \times 0.1$ m, with one muscle layer with a spherical tumor inside, as described in Fig. 2. The OcTree mesh is shown in Fig. 3. It was constructed with 68,839 cubic volumes of edge sizes 0.00078125 m,

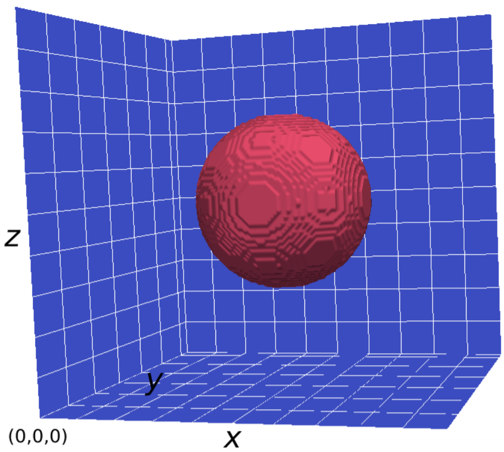

Figure 2: Domain of the numerical experiment. Layer of muscle and tumor in the form of sphere.

0.0015625 m, 0.003125 m and 0.00625 m. As can be seen from the Fig. 3, the constructed OcTree mesh is able to describe the geometry of the tumor with good resolution and, at the same time, it greatly reduces the number of volumes. In this sense, a regular mesh to represent this same geometry with equivalent resolution would be require 2,097,152 control volumes with edge size 0.00078125 m, which is more than 30 times the number of degrees of freedom presented in the OcTree mesh.

Regarding boundary conditions, at the border representing the interior of the body, a temperature of $\phi = 37^o$ C is prescribed in order to simulate the core temperature, while null heat fluxes are prescribed in the remaining boundaries. The arterial temperature ϕ_a is also set to 37^o C. The parameter values were taken from the literature (Lang et al., 1999; Minkowycz,

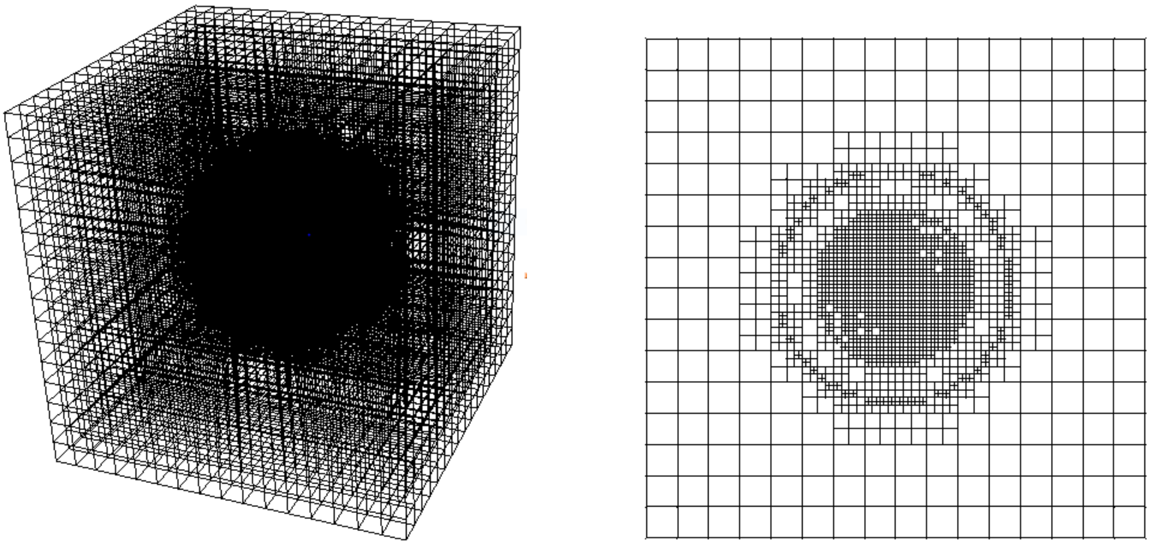

(a) (b)

Figure 3: Octree mesh with 68,839 control volumes with four different sizes:(a) 3D Mesh; (b) Slice at $y = 0.05m$.

2009; Loureiro et al., 2014; Reis et al., 2016) and are presented in Table 1. Concerning the heat source, the position for the injection of nanoparticles are $(0.05\text{m}, 0.05\text{m}, 0.05\text{m})$ and the parameters $A = 3.3 \times 10^6$ W/m^3 and $r_0 = 2.4 \times 10^{-3}$.

Table 1: Model parameters

Symbol	Unit	Muscle	Tumor
Q_m	W/m^3	420.0	4200.0
c	J/Kg^{o}C	3800.0	4200.0
c_b	J/Kg^{o}C	4200.0	4200.0
κ	W/m^{o}C	0.45	0.55
ρ	Kg/m^3	1000.0	1000.0
W_b	Kg/s/m^3	1.8789	0.7579

To determine the initial condition, the steady-state regime problem was solved without Q_r (here only Q_m is considered). The non-symmetrical system of equations obtained by the FVM is solved by the biconjugate gradient stabilized solver. Figure 4 shows the temperature field along with a slice passing at the center of the sphere ($y = 0.05$ m) of the computed initial condition. Recall that in the adopted FVM, the temperature is constant over each control volume and all slice figures of the temperature field are henceforth presented without any interpolation procedure.

The numerical schemes was employed to simulate the same physical phenomenon, using the explicit method named "Exp" using the OcTree mesh with four different sizes of control volumes. For comparison purposes, the other scheme named "Ref" based on the use of a regular

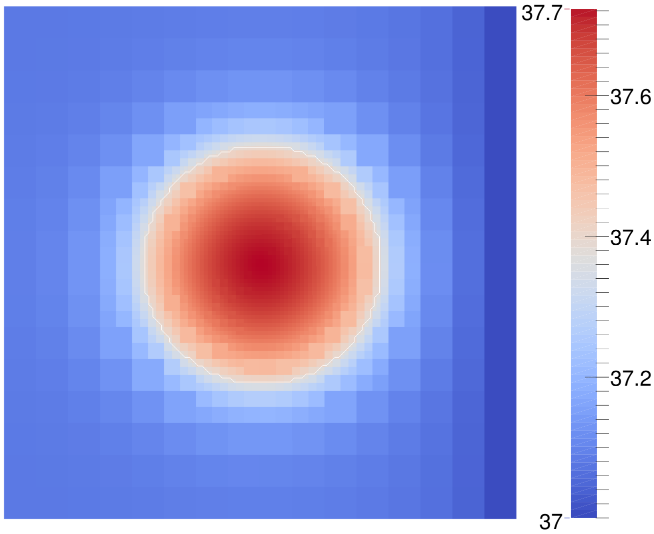

Figure 4: Slice at $y = 0.05$ m of the initial condition obtained by the steady–state solution.

conforming mesh with grid spacing corresponding to the smallest edge size of the OcTree mesh is also employed. The last scheme is a complete equivalence of the finite volume method with the finite difference method with staggered-grid (Dormy and Tarantola, 1995). Actually, it has complete equivalence with the so-called equivalent staggered-grid scheme, a scheme formulated using only one field (temperature in this case) that considers implicitly the fluxes (Di Bartolo et al., 2012; Di Bartolo et al., 2015; Di Bartolo et al., 2017).

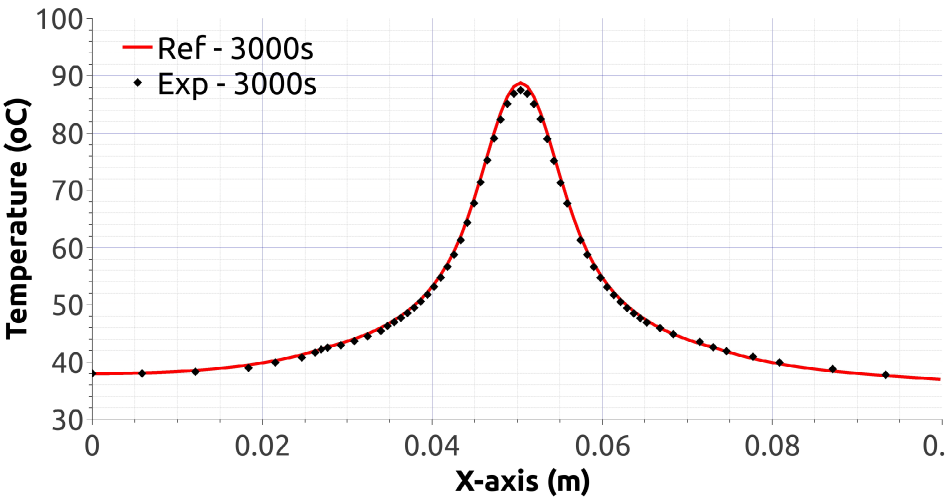

Figure 5: Comparison between the solution of the Octree mesh modeling considering the Reference and explicit schemes.

The numerical parameters adopted are $\Delta t = 0.75$ s. As shown in Fig. 5, the explicit and reference formulation yielded very close results as can be seen by profiles at $t = 3000$ s in a straight line in the x-axis direction with $y = 0.05$ m and $z = 0.05$ m. Figure 6 shows the temperature variation with respect to the time at point (0 m, 0.05 m, 0.05 m), comparing the two schemes.

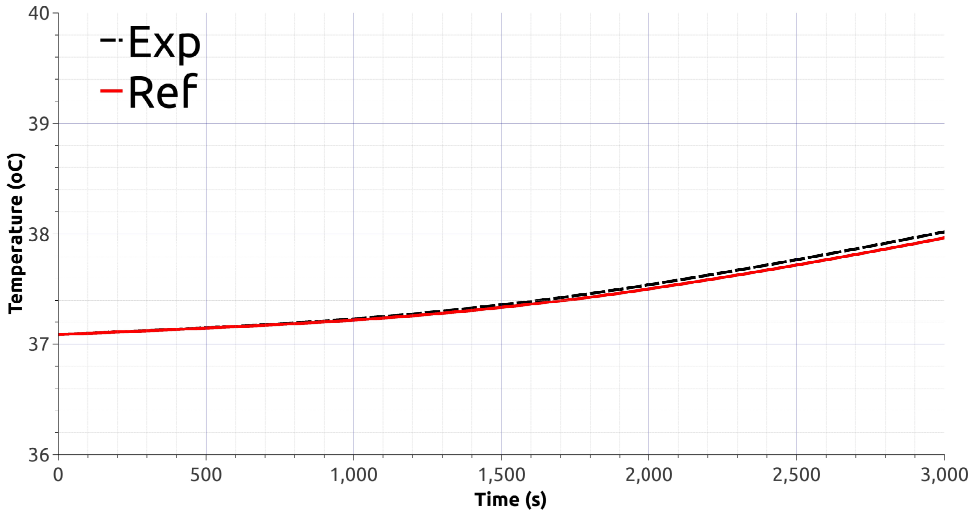

Figure 6: Temperature variation with respect to the time at the point (0, 0.5, 0.5).

A set of snapshots of the temperature field at some times on xz plane with $y = 0.05$ m and $y = 0.066$ m are presented in Fig. 7 and Fig. 8 comparing both the Exp and Ref schemes in order to show the heat diffusion across the tumor. Bearing in mind that the rate of human cell viability decay rapidly with increasing temperature and exposure time (Feng et al., 2008), an isothermal line (black line) of 43^oC is also plotted to better visualize the region over which the cells are probably damaged. The white line, on the other hand, shows the boundary (shape) of the tumor in the sliced figure.

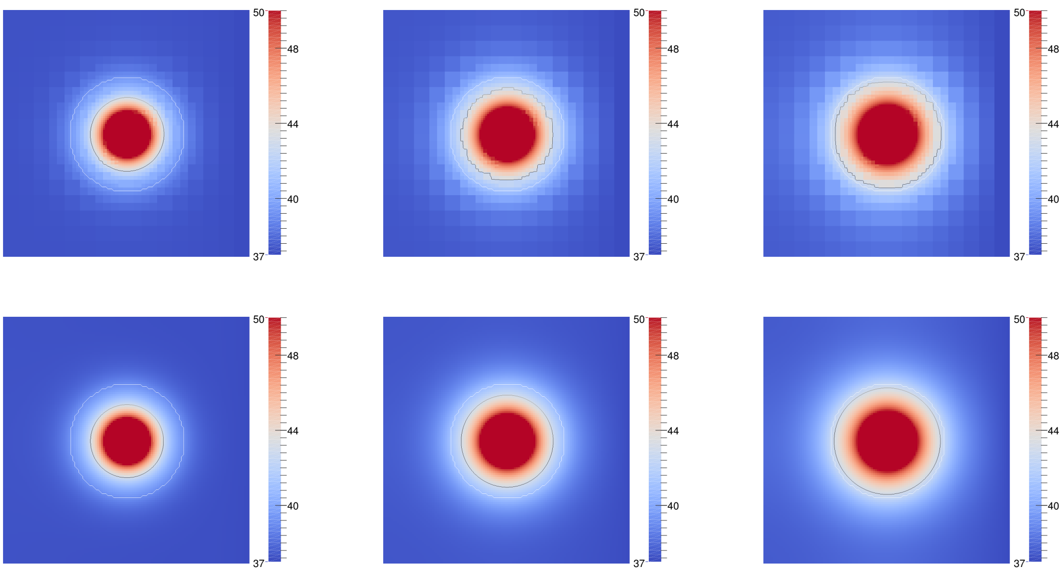

Figure 7: Slices at $y = 0.05$ m for the schemes Exp (above) and Ref (below) at times 1000 s (left), 2000 s (middle), and 3000 s (right). The white line determines the tumor contour and the black, the 43^oC isotherm.

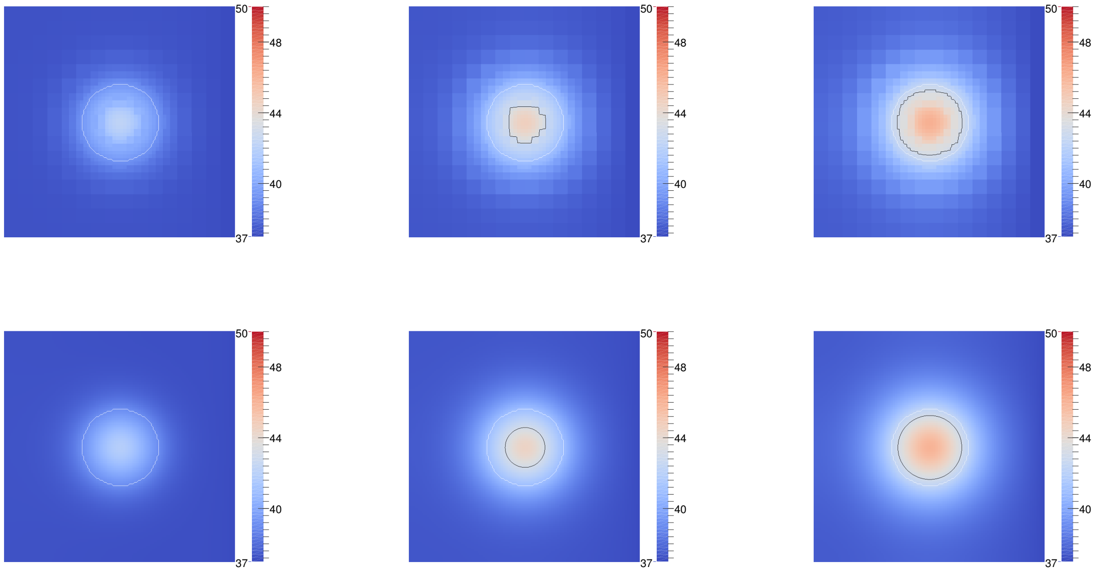

Figure 8: Slices at $y = 0.066$ m for the schemes Exp (above) and Ref (below) at times 1000 s (left), 2000 s (middle), and 3000 s (right). The white line determines the tumor contour and the black, the 43^oC isotherm.

5 CONCLUSIONS

A 3D numerical simulation of an innovative hyperthermia treatment were presented. The hyperthermia with nanoparticles can be used as a non-invasive treatment for destroying tumors in living tissue. The goal is to heat the tumor up to a temperature threshold above the normal physiological one in order to destroy its cells by necrosis while maintaining the damage of the healthy tissue as minimal as possible. This process was mathematically modeled by considering Pennes' bioheat equations that describe the heat transfer in living tissue. The FVM was applied using OcTree meshes for spatial discretization. The developed scheme has some advantages in comparison to those using regular grid and unstructured mesh. The OcTree is relatively easy to generate in comparison to unstructured meshes and, at the same time, it allows local refinement. In this sense, the OcTree mesh is a good compromise between precision and CPU time, avoiding the complexity of algorithms using completely unstructured mesh.

At the present stage, the developed algorithm was applied to a simple domain contained by a homogeneous living tissue with a spherical tumor. The results obtained are very similar to the FDM using refined grid, with the advantage to using much less unknows and hence the proposed scheme is more efficient. The scheme is very promising specially due to the possibility of local refinement, important for good geometrical representation of the tumor and tissues, as well as for capturing more precisely the temperature variations due to high gradients as, for instance, those around concentrated sources. In addition, the nonconforming mesh is readily incorporated into the FVM through the flux balance on the faces; a characteristic not encountered in other numerical methods such as the finite element method in which a more complex formulation (discontinuous finite element approaches) needs to be taken into account.

The example presented in this work leads to a great reduction in the number of degrees of freedom in comparison to regular grids. In fact, comparing the use of an OcTree mesh with a regular grid, a speedup of 30 was achieved without degrading the accuracy. Finally, it is noteworthy that the numerical efficiency is a crucial issue to be considered when solving optimization problems, that can be used to guide the specialist in real-time during the medical procedure, improving the treatment results and security.

ACKNOWLEDGMENTS

This work was partially supported by CNPq and FAPEMIG. L. Di Bartolo especially appreciates the efforts of the last two elected presidents to support research and education in Brazil.

REFERENCES

T. J. Barth. *Aspects of unstructured grids and finite-volume solvers for the Euler and Navier-Stokes equations*. Agard repo edition, 1992.

K. Das and S. C. Mishra. Estimation of tumor characteristics in a breast tissue with known skin surface temperature. *J. Therm. Biol.*, 38(6):311–317, 2013. ISSN 0306-4565. doi: 10.1016/j.jtherbio.2013.04.001. URL `http://dx.doi.org/10.1016/j.jtherbio.2013.04.001`.

K. Das and S. C. Mishra. Non-invasive estimation of size and location of a tumor in a human breast using a curve fi tting technique ? *Int. Commun. Heat Mass Transf.*, 56: 63–70, 2014. ISSN 0735-1933. doi: 10.1016/j.icheatmasstransfer.2014.04.015. URL `http://dx.doi.org/10.1016/j.icheatmasstransfer.2014.04.015`.

K. Das, R. Singh, and S. C. Mishra. Numerical analysis for determination of the presence of a tumor and estimation of its size and location in a tissue. *J. Therm. Biol.*, 38(1):32–40, 2013. ISSN 0306-4565. doi: 10.1016/j.jtherbio.2012.10.003. URL `http://dx.doi.org/10.1016/j.jtherbio.2012.10.003`.

L. Di Bartolo, C. Dors, and W. Mansur. A new family of finite-difference schemes to solve the heterogeneous acoustic wave equation. *Geophysics*, 77(5):T187–T199, 2012. doi: 10.1190/geo2011-0345.1. URL `https://doi.org/10.1190/geo2011-0345.1`.

L. Di Bartolo, C. Dors, and W. J. Mansur. Theory of equivalent staggered-grid schemes: application to rotated and standard grids in anisotropic media. *Geophys. Prospect.*, 2015. doi: 10.1111/1365-2478.12210. URL `https://doi.org/10.1111/1365-2478.12210`.

L. Di Bartolo, L. Lopes, and L. J. R. Lemos. High-order FD approximations to solve pseudo-acoustic equations in 3D VTI media. *Geophysics*, 82(5):T225–T235, 2017.

E. Dormy and A. Tarantola. Numerical simulation of elastic wave propagation using a finite volume method. *Journal of Geophysical Research: Solid Earth (1978–2012)*, 100(B2):2123–2133, 1995.

Y. Feng, J. Tinsley Oden, and M. N. Rylander. A Two-State Cell Damage Model Under Hyperthermic Conditions: Theory and In Vitro Experiments. *J. Biomech. Eng.*, 130(4):041016, 2008. ISSN 01480731. doi: 10.1115/1.2947320.

H. Gwon. International Journal of Heat and Mass Transfer Numerical analysis for the conjugate heat transfer of skin under contrast therapy. *Int. J. Heat Mass Transf.*, 86: 388–396, 2015. ISSN 0017-9310. doi: 10.1016/j.ijheatmasstransfer.2015.03.019. URL `http://dx.doi.org/10.1016/j.ijheatmasstransfer.2015.03.019`.

E. Haber and S. Heldmann. An octree multigrid method for quasi-static Maxwell's equations with highly discontinuous coefficients. *J. Comput. Phys.*, 223(2):783–796, 2007.

L. Horesh and E. Haber. A second order discretization of maxwell's equations in the quasi-static regime on octree grids. *SIAM Journal on Scientific Computing*, 33(5):2805–2822, 2011.

S. Huang and J. Hainfeld. Intravenous magnetic nanoparticle cancer hyperthermia. *International Journal of Nanomedicine*, pages 2521–2532, 2013.

J. Lang, B. Erdmann, and M. Seebass. Impact of nonlinear heat transfer on temperature control in regional hyperthermia. *IEEE Transactions on Biomedical Engineering*, 46(9):1129–1138, 1999.

F. Loureiro, W. Mansur, L. Wrobel, and J. Silva. The explicit greens approach with stability enhancement for solving the bioheat transfer equation. *International Journal of Heat and Mass Transfer*, 76:393–404, 2014.

W. Minkowycz. *Advances in numerical heat transfer*, volume III. CRC press, 2009.

W. Minkowycz, E. M. Sparrow, and J. P. Abraham. *Nanoparticle heat transfer and fluid flow*. CRC press, 2012.

S. Nóbrega and P. J. Coelho. A parametric study of thermal therapy of skin tissue. *J. Therm. Biol.*, 63(November 2016):92–103, 2017. ISSN 0306-4565. doi: 10.1016/j.jtherbio.2016.11.016. URL `http://dx.doi.org/10.1016/j.jtherbio.2016.11.016`.

S. Popinet. Gerris: A tree-based adaptive solver for the incompressible Euler equations in complex geometries. *J. Comput. Phys.*, 190(2):572–600, 2003.

J. N. Reddy. *An Introduction to Nonlinear Finite Element Analysis: with applications to heat transfer, fluid mechanics, and solid mechanics*. OUP Oxford, 2014.

R. F. Reis, F. S. Loureiro, and M. Lobosco. 3D numerical simulations on GPUs of hyperthermia with nanoparticles by a nonlinear bioheat model. *J. Comput. Appl. Math.*, 295:35–47, 2016. ISSN 03770427. doi: 10.1016/j.cam.2015.02.047. URL `http://dx.doi.org/10.1016/j.cam.2015.02.047`.

M. Salloum, R. Ma, and L. Zhu. An in-vivo experimental study of temperature elevations in animal tissue during magnetic nanoparticle hyperthermia. *Int. J. Hyperth.*, 24(7):589–601, 2008. doi: 10.1080/02656730802203377. URL `http://dx.doi.org/10.1080/02656730802203377`.

A. Valente, L. Di Bartolo, and W. Mansur. 3D octree finite-volume method for acoustic wave simulation. In *Anais do 36 Cilamce*, Rio de Janeiro, Brasil, November 2015a.

A. G. Valente, L. Di Bartolo, and W. J. Mansur. 3D seismic modeling using staggered-grid OcTree mesh. In *SEG Tech. Progr. Expand. Abstr.*

2015, pages 3754–3758, 2015b. doi: 10.1190/segam2015-5882491.1. URL https://doi.org/10.1190/segam2015-5882491.1.

S. C. J. Æ. X. X. Zhang. Dynamic modeling of photothermal interactions for laser-induced interstitial thermotherapy : parameter sensitivity analysis. *Lasers Med. Sci.*, 20(3):122–131, 2005. doi: 10.1007/s10103-005-0359-5.

O. C. Zienkiewicz and K. Morgan. *Finite Element and Approximation*. John wiley edition, 1983.